Reflectivity of a disordered monolayer estimated by graded refractive index and scattering models

Ruth Diamant,[1,*] Augusto Garcí-Valenzuela,[2] and Manuel Fernández-Guasti[1]

[1]*Laboratorio de Óptica Cuántica, Departamento de Física, Universidad A. Metropolitana—Iztapalapa, 09340 México D.F., Ap. postal 55-534, Mexico*

[2]*Centro de Ciencias Aplicadas y Desarrollo Tecnológico, Universidad Nacional Autónoma de México, Ap. postal 76-186, D. F., Mexico*

**Corresponding author: ruth@xanum.uam.mx*

Received June 19, 2012; revised July 20, 2012; accepted July 21, 2012; posted July 23, 2012 (Doc. ID 170875); published August 21, 2012

Reflectivity of a random monolayer, consisting of transparent spherical particles, is estimated using a graded refractive index model, an effective medium approach, and two scattering models. Two cases, a self-standing film and one with a substrate, are considered. Neither the surrounding medium nor the substrate are absorbing materials. Results at normal incidence, with different particle sizes, covering ratios and refractive indexes, are compared. The purpose of this work is to find under which circumstances, for reflectivity at normal incidence, a particle monolayer behaves as a graded refractive index film.

OCIS codes: 290.5850, 310.6860, 240.0310, 290.4210, 290.1350, 310.6628.

1. INTRODUCTION

The optical properties of small particle monolayers have been of interest for many years now. Many works have explored the determination of structural information from optical reflectivity or transmissivity measurements [1,2]. When particles are very small compared to the wavelength of light, so that there is very little scattering, the reflectivity has traditionally been modeled using an effective layer approach [1–7]. In these studies, an effective permittivity and thickness for an artificial equivalent film is derived, or an effective surface susceptibility for an equivalent plane that mimics the reflectivity of the disordered monolayer is formulated. The effective layer or equivalent plane turns out to be optically anisotropic and thus the effective electric permittivity or surface susceptibility is a tensor. To our knowledge, an "equivalent stratified or graded layer" has not yet been proposed to model monolayer light reflection. We intend to do that for normal incidence, i.e., incident light traveling perpendicularly to the layer plane. Comparison with two scattering models and an effective medium approach is made to find under which circumstances a particle monolayer behaves as a graded refractive index film.

For the scattering models, both the Mie solution and the Rayleigh–Gans approximation are used. The first scattering model is a single-scattering one, no interaction among scatterers is considered; the second is a recently developed multiple-scattering model (MSM) that includes some of this interaction [8]. The effective medium approach simply replaces the spheres with a homogeneous film having a constant refractive index, a spatial average for all the monolayer, while the graded refractive index model replaces the spheres with a stratified film by averaging the refractive index over surfaces parallel to the monolayer. Light propagation through an inhomogeneous film is handled with an amplitude and phase representation scheme also recently proposed [9]. The purpose of this work is to find under which circumstances a particle monolayer behaves as a graded refractive index film, for normal incidence.

For simplicity, here we will consider only monolayers of identical spherical particles of radius a and refractive index n_2. A free standing monolayer consists of an ensemble of N particles embedded in a homogenous medium of refractive index n_1, placed randomly on a plane as depicted in Fig. 1. It is assumed that the particle centers lie on the plane; we place this plane at $z = -a$. A monolayer of infinite extent assumes that its area A as well as N tend to infinity but their ratio, the so-called surface density of particles $\rho = N/A$ remains constant. The surface covering ratio is $\Theta = N\pi a^2/A$, the area fraction covered by particles as viewed in a direction perpendicular to the monolayer. If a substrate, with different refractive index n_3, is present, its boundary will be placed at $z = 0$. Incident light will be plane monochromatic waves, of wavelength λ, arriving from the negative side of the z axis.

An equivalent graded layer (EGL) is expected to be accurate for low contrast and rather small particles; on the other hand, scattering models are reliable for small surface covering ratios. In Table 1, the ranges for n_1, n_2, n_3, Θ, and a used in this work are presented.

A. The Scattering Models

1. One Isolated Scattering Element

For any choice of approximation, the amplitude of the field scattered by a particle is a linear function of the amplitude of the incident field. The relation between incident and scattered fields is conveniently written in the matrix form [10,11]

$$\begin{pmatrix} E_{\parallel}^{S} \\ E_{\perp}^{S} \end{pmatrix} = \frac{e^{ik_0(r-z)}}{-ik_0 r} \begin{pmatrix} S_2 & S_3 \\ S_4 & S_1 \end{pmatrix} \begin{pmatrix} E_{\parallel}^{i} \\ E_{\perp}^{i} \end{pmatrix}, \tag{1}$$

where $E_{\parallel}$ and $E_{\perp}$ indicate polarization directions relative to the scattering plane, and $\mathbf{r}$ is the position vector of the

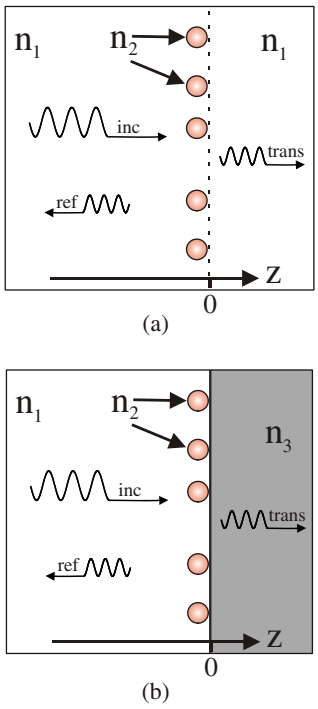

Fig. 1. (Color online) Monolayer in both cases, (a) without and (b) with a substrate. Refractive indexes n_1, n_2, and n_3 belong to the surrounding medium, spheres, and substrate, respectively. The curly arrows represent incident, reflected, and transmitted light. Scattered light is not shown.

observation point relative to the scatterer, so r is its magnitude and z is its component along the propagation direction of the incident plane wave. $S_j (j = 1, 2, 3, 4)$ are the amplitude scattering matrix elements, which in general are functions of θ and ϕ, the axial an azimuthal angles of the **r** vector. Finally, k_0 is the wavenumber in vacuum. In particular, for a sphere, the amplitude scattering matrix elements S_1 and S_2 depend only on θ and $S_3 = S_4 = 0$.

These matrix elements can be computed using the Mie solution, or the Rayleigh or the Rayleigh–Gans approximations.

Mie scattering. Mie scattering by a sphere is obtained after solving Maxwell equations subjected to particular boundary conditions; it is expressed in terms of infinite series. To write the amplitude scattering matrix elements for the Mie solution is rather elaborate; it involves Legendre polynomials and spherical Bessel and Henkel functions. Moreover, finding analytic solutions for particles of arbitrary shape could be a very difficult challenge [12]. The Mie Solution is valid for a spherical scatterer of any size, yet computation of the scattering fields produced by rather large spheres may need a lot of terms to converge; in that case it may be more convenient to use geometrical optics. In the other limiting case, for small spherical particles compared to the wavelength, there are more simple approximations such as Rayleigh scattering or the so-called Rayleigh–Gans theory. Presently, software to perform electromagnetic scattering simulations based on classical Mie theory can be found on the Web [13].

Table 1. Ranges for Radii, Refractive Indexes, and Surface Covering Ratios

Parameter	n_1	n_2	n_3	Θ	a
Range	1	1.1 to 1.5	1.5	0.1 to 0.3	0 to 1λ

Rayleigh scattering. Rayleigh scattering of electromagnetic radiation assumes particles much smaller than the wavelength of the light. The simplification introduced by the size smallness is that the scatterer may be considered as a point source, placed in a homogeneous electric field and radiating like a single dipole.

Rayleigh–Gans approximation. Rayleigh–Gans approximation includes a wider range of particle sizes, such that $\left|\frac{n_2}{n_1} - 1\right| \ll 1$ and $2ak\left|\frac{n_2}{n_1} - 1\right| \ll 1$, where k is the wavenumber [10,11]. We may interpret these conditions as the requirement that the incident wave does not undergo appreciable change of phase or amplitude when it enters the particle. The basis for the Rayleigh–Gans approximation is ordinary Rayleigh scattering; every small volume element of the particle is considered as an independent Rayleigh scatterer. Each volume element is excited by the incident wave that travels almost undisturbed through the particle. Interference in the far field by all these volume elements will determine the scattering amount in that direction.

To write the amplitude scattering matrix elements for the Rayleigh–Gans approximations is simple,

$$S_1 = -ix_m^3\left(\frac{n_2^2 - n_1^2}{n_2^2 + 2n_1^2}\right)\mathfrak{f}(\theta), \tag{2}$$

$$S_2 = -ix_m^3\left(\frac{n_2^2 - n_1^2}{n_2^2 + 2n_1^2}\right)\mathfrak{f}(\theta)\cos\theta, \tag{3}$$

where $x_m \equiv n_1 k_0 a$ is the size parameter of the particle and $\mathfrak{f}(\theta) = \frac{3}{u^3}(\sin u - u\cos u)$ is the form factor; here $u = 2x_m \sin\frac{\theta}{2}$. If the form factor is substituted by unity, the matrix elements correspond to those for Rayleigh scattering. When $n_2 \approx n_1$, it is customary to express the former matrix elements using $\frac{n_2^2 - n_1^2}{n_2^2 + 2n_1^2} \approx \frac{2}{3}\left(\frac{n_2}{n_1} - 1\right)$. For particles of arbitrary shape, these small particle approximations may lead to conveniently simple expressions too.

2. Collective Phenomena

The scattering of light by a collection of particles is based on what is known about the scattering by one particle.

SSA for a monolayer. The simplest scattering model often used to calculate the optical reflectivity from low-density random monolayers of particles is the single-scattering approximation (SSA). In this approximation, one assumes that the electromagnetic wave incident on the particles (the exciting field) is the incident wave and ignores direct interaction among the particles. Let us recall that the reflectivity of a surface is obtained experimentally by dividing the optical power of the specularly reflected light with that of the incident beam. From the theoretical side, the reflectivity of a disordered monolayer of particles is well approximated by the magnitude square of the reflection coefficient of the average wave. The average is taken over all permitted configurations of the particulate system weighted by the probability of each configuration. The power carried by the average wave is commonly referred to the coherent component of the scattered light, and in the case of a plane monolayer of particles, the coherent

component of the reflected light travels only in the specular direction [8]. When particle sizes are comparable to the wavelength of light, in addition to the coherent component there is also a diffuse component of light that carries optical power in all directions. When particles are very small compared to the wavelength, the diffuse component of the scattered light carries a small amount of power compared to that of the coherent component and may be ignored. The coherent reflection and transmission coefficients are obtained by averaging the fields scattered by the particles in the reflection and transmission hemispheres. The resulting coherent reflection and transmission coefficients for spherical particles are given by [14]

$$r_{\mathrm{coh}}^{\mathrm{SSA}} = -\alpha S_j(\pi - \theta_i), \tag{4}$$

$$t_{\mathrm{coh}}^{\mathrm{SSA}} = 1 - \alpha S_j(0). \tag{5}$$

Here $\alpha = 2\Theta/x_m^2 \cos\theta_i$, where θ_i is the incidence angle. The function $S_j(\theta)$ is an element of the amplitude scattering matrix of an isolated spherical particle of radius a and refractive index n_2 embedded in a homogenous medium of refractive index n_1. In particular, for normal incidence, $\theta_i = 0$. The main advantage of the SSA is its simplicity, which among other things allows for direct physical insight into reflectivity of a sparse, random monolayer of particles. However, it is known that the SSA can incur in large relative-errors for the coherent transmittance of a low-density monolayer of very small particles [8,14], although it can be accurate in calculating the coherent reflectance. The factor α has the function $\cos\theta_i$ in the denominator, so the reflection and transmission coefficients in Eqs. (4) and (5) diverge when $\theta_i \to \pi/2$. This means that the SSA is limited to low angles of incidence.

MSM for a monolayer. In order to improve over these limitations it is necessary to incorporate the effects of multiple scattering among the particles into the model. When particles are not small enough and scattering by them is important, a suitable approach to calculate the reflectivity signal is using coherent scattering models [8,15]. By coherent scattering approach we mean to solve the multiple-scattering problem and calculate the average scattered wave. Coherent scattering models must incur in some approximations in order to be of practical use. In [15], a new model taking into account some multiple scattering was developed. However, the derivation of the model was somewhat heuristic, thus casting some uncertainty on the validity of the resulting model. Recently, an MSM was derived using a rigorous multiple-scattering formalism [8]. The MSM provides closed-form expressions for the coherent reflection and transmission coefficient of a monolayer of spherical particles. Basically, an integral equation for the average field exciting the particles in the monolayer is setup under the so-called quasi-crystalline approximation (QCA). Then, this equation is solved approximately assuming the average exciting field is given by two plane waves traveling in the incident and specular directions, respectively. Once the exciting field is known, the average scattered electromagnetic waves in the transmission and reflection directions are calculated, and from their amplitude the coherent reflection and transmission coefficients are obtained. These coefficients can be written as

$$r_{\mathrm{coh}}^{\mathrm{MSM}} = \frac{-\alpha S_j(\pi - \theta_i)}{1 + \alpha S_j(0) + \frac{\alpha^2}{4}[S_j^2(0) - S_j^2(\pi - 2\theta_i)]}, \tag{6}$$

$$t_{\mathrm{coh}}^{\mathrm{MSM}} = \frac{1 - \frac{\alpha^2}{4}[S_j^2(0) - S_j^2(\pi - 2\theta_i)]}{1 + \alpha S_j(0) + \frac{\alpha^2}{4}[S_j^2(0) - S_j^2(\pi - 2\theta_i)]}. \tag{7}$$

The coefficients in Eqs. (6) and (7) are expected to be accurate for monolayers with moderately small surface covering ratios, but, if based on the Mie solution, the radius of the particles, their refractive index, and the angle of incidence are unrestricted. Again, for normal incidence, $\theta_i = 0$.

B. Reflectivity of a Monolayer Supported by a Flat Surface

Let us assume a monolayer of spherical particles sitting on top of a flat surface and a plane wave incident on the system at an angle θ_i; the average or coherent wave gets partly reflected and partly transmitted by the monolayer. Part of the transmitted coherent wave gets reflected again on the substrate surface. Each time the average wave is incident on the monolayer from the substrate, it gets partly reflected and partly transmitted. Adding the initially reflected wave and all the waves partly transmitted back into the incidence medium, due to the multiple reflections, gives the coherent reflection coefficient for the supported monolayer (r_{supp})

$$r_{\mathrm{supp}}(\theta_i) = r_{\mathrm{coh}}(\theta_i) + \frac{r_s(\theta_i) t_{\mathrm{coh}}^2(\theta_i) e^{i\beta}}{1 - r_s(\theta_i) r_{\mathrm{coh}}(\theta_i) e^{i\beta}}, \tag{8}$$

where r_s is the reflection coefficient of the underlying surface supporting the monolayer, evaluated at an angle of incidence θ_i, $\beta = 2x_m \cos\theta_i$ is the phase difference between successive reflections of the coherent wave between the monolayer's plane and the underlying surface, and r_{coh} and t_{coh} are the coherent reflection and transmission coefficients of the free standing monolayer. In this assumption the monolayer acts as an effective interface, standing at a distance a from the substrate.

C. Reflectivity of a Thin Homogeneous Film (THF)

The simplest model formulation for a monolayer is to replace it with a homogeneous film. Traditionally, the Maxwell Garnett equation is used to determine the effective refractive index of a medium consisting of spherical inclusions with n_2 embedded in a matrix with $n_1 = 1$ [11]:

$$n_{\mathrm{eff}}^2 = 1 + \frac{3f\left(\frac{n_2^2 - 1}{n_2^2 + 2}\right)}{1 - f\left(\frac{n_2^2 - 1}{n_2^2 + 2}\right)}, \tag{9}$$

where f is the volume fraction and the substitution $\varepsilon = n^2$ has been made. Using Eq. (9) and expanding n_{eff} in a Taylor series as a function of n_2, around $n_2 = 1$, yields

$$n_{\mathrm{eff}} \approx f(n_2 - 1) + 1, \tag{10}$$

which corresponds to the volume average of the refractive index. For the ranges of surface covering ratios Θ and particle

refractive indexes n_2 considered in this work (Table 1), Eq. (10) leads to very similar refractive index values as Eq. (9); the difference never exceeds 3%. For simplicity, let us use the film's refractive index average $n_{\text{avg}} = f(n_2 - 1) + 1$ as the effective one. In our case, $f = \frac{2}{3}\Theta$.

Reflectivity for a thin film on a substrate is [16]

$$R = 1 - \frac{(r_{12}r_{23} + 1)^2 - (r_{12} + r_{23})^2}{(r_{12}r_{23} + 1)^2 - 4r_{12}r_{23}\sin^2(k_0 n_{\text{avg}} 2a)}, \tag{11}$$

where $r_{12} = \frac{n_{\text{avg}} - n_1}{n_{\text{avg}} + n_1}$ and $r_{23} = \frac{n_3 - n_{\text{avg}}}{n_3 + n_{\text{avg}}}$. If there is no substrate, $n_3 = n_1 = 1$.

2. REFLECTIVITY OF A THIN LAYER WITH A CONTINUOUS BUT VARYING REFRACTIVE INDEX, AN EQUIVALENT GRADED LAYER (EGL)

The processes of transmission, reflection, and refraction are macroscopic manifestations of scattering occurring on a microscopic level [17]. Molecules that make up a transparent solid material behave like Rayleigh scatterers that interfere strongly with each other, so close together and so small compared to the wavelength (of visible light) that we can treat matter as a continuum. Let us use a differential volume big enough to see matter as a continuum but small enough to account for permittivity changes as a function of one direction in space.

As with the THF, let us again simply average the monolayer refractive index $n(\mathbf{r})$, but this time along planes perpendicular to the z axis. Take any plane parallel to the xy plane between $z = -2a$ and $z = 0$; let p be the surface fraction of this plane with a refractive index n_2. For this z range, $n(z) = pn_2 + (1 - p)n_1$. Consider one particle (see Fig. 2); the plane intersects the particle yielding a circular slice of radius $d(z)$, and then $p(z) = \pi d^2 \rho$, where $d^2 = a^2 - (z + a)^2$ and $\rho = \frac{\Theta}{\pi a^2}$. Now the graded refractive index for every z value can be written as

$$n(z) = \begin{cases} n_1 & \text{for } z \le -2a \\ n_1 + \Theta(n_2 - n_1)\left[1 - \left(\frac{z}{a} + 1\right)^2\right] & \text{for } -2a < z < 0 \\ n_3 & \text{for } z \ge 0 \end{cases}. \tag{12}$$

If $n_3 = n_1$, there is no substrate. Some examples of $n(z)$ plots are shown in Fig. 3.

A plane monochromatic wave, with its electric field vector parallel to the x axis, is incident normally on the stratified medium. In this case, the second-order differential equation that describes the electric field is nonautonomous due to the dependence of permittivity and/or permeability on the spatial z coordinate [16]:

$$\frac{d \ln \mu}{dz}\frac{\partial E_x}{\partial z} = k_0^2 n^2 E_x + \left(\frac{\partial^2 E_x}{\partial y^2} + \frac{\partial^2 E_x}{\partial z^2}\right). \tag{13}$$

For normal incidence, E_x depends only on z and if the media are nonmagnetic $\mu = 1$, Eq. (13) can be simplified to

$$0 = k_0^2 n^2 E_x + \frac{\partial^2 E_x}{\partial z^2}. \tag{14}$$

The electric field $E_x(z)$ is a complex function of z and can be recast in terms of its amplitude and phase: $E_x = Ae^{iq}$, where A and q are real functions of z. Equations for the amplitude A and phase q can be decoupled but an invariant Q still relates both quantities [9,18]:

$$A'' - \frac{Q^2}{A^3} = -k_0^2 n^2 A, \tag{15}$$

$$A^2 q' = Q. \tag{16}$$

Equation (15) is of the Ermakov–Pinney type, and Eqs. (14) and (15) constitute an Ermakov pair; their solutions are

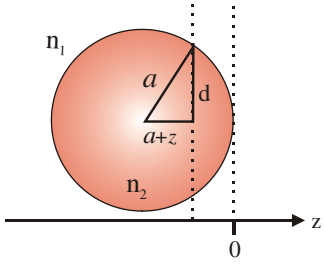

Fig. 2. (Color online) Consider one particle and any plane perpendicular to the z axis between $z = -2a$ and $z = 0$.

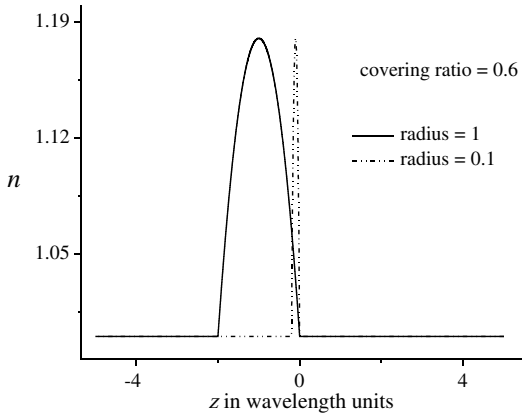

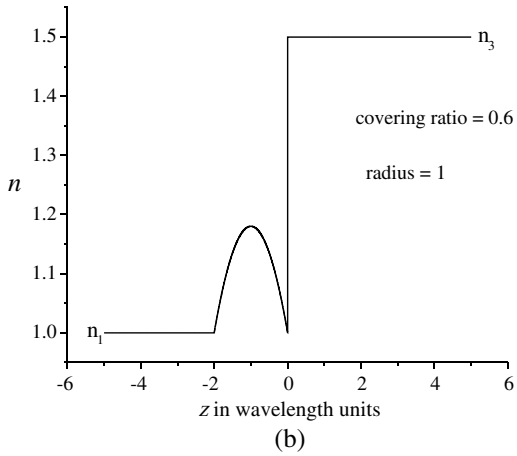

Fig. 3. $n(z)$ in both cases, (a) without and (b) with a substrate.

closely related [19,20]. Solutions for Eq. (15), when $n(z)$ is an arbitrary but a bounded function of z, can be found numerically [21]. Establishing convenient initial conditions so that light is only transmitted to the right of the z axis, meaning that incident light only arrives from the left (negative) side, the amplitude reflection coefficient $r = \sqrt{R}$ can be inferred from solution's local maxima and minima [9,18]:

$$r = \frac{A_{\text{reflected}}}{A_{\text{incident}}} = \frac{A_{\max} - A_{\min}}{A_{\max} + A_{\min}}. \tag{17}$$

For our purposes, this amplitude and phase representation method is a more suitable alternative to the transfer matrix method as no approximation is needed regarding how abruptly or softly the refractive index varies compared to the wavelength. Also, the squared amplitude A^2 is directly related to light intensity, which is usually the measured physical quantity.

3. REFLECTIVITY RESULTS

A. Comparison with Scattering Models Using the Mie Solution

1. Free Standing Monolayer

Reflectivity was calculated for monolayers with different particle radii a, refractive indexes n_2, and covering ratios Θ, using the SSA, MSM, EGL, and THF models. In this section, the scattering models were based on the Mie solution and its amplitude scattering matrix elements. The surrounding medium refractive index is always $n_1 = 1$.

Reflectivity versus radius plots are the graphs that exhibit more clearly the coincidence range among models. In Fig. 4(a), a typical graph is displayed for a monolayer with refractive index $n_2 = 1.3$ and covering ratio $\Theta = 0.3$. Within the interval $a < 0.1\lambda$, all four reflectivity predictions are very close. Then, for $a > 0.1\lambda$, the THF solution departs from the rest; it oscillates periodically between constant maxima and minima values. The radii difference between critical points is $\Delta a = \frac{1}{8n_{\text{avg}}}\lambda$. In contrast, the reflectivity for the scattering models and EGL keeps rising beyond $a \approx 0.1\lambda$, reaching a higher maximum at $a \approx 0.16\lambda$. The value of this maximum is slightly different for each model, but all three of them behave similarly up to $a \approx 0.3\lambda$, that is for more than half a wavelength in diameter. For greater radii, all the solutions oscillate but the height and/or width of these oscillations is not the same. The SSA presents higher reflectivity than the MSM, but maxima and minima are coincident for the horizontal coordinate (same radii); their oscillation period is somewhat smaller compared to the THF. Within this range, reflectivity for EGL is even lower but the oscillation period is very similar to that predicted by the THF, although extrema do not fall

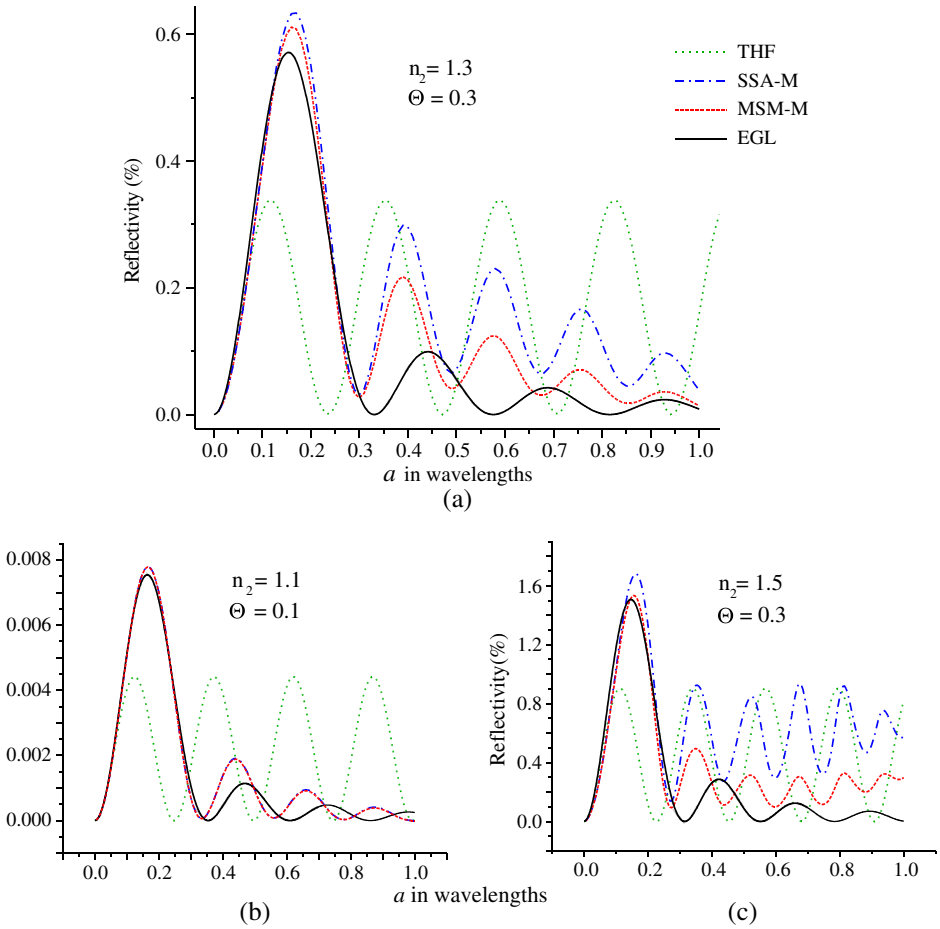

Fig. 4. (Color online) Reflectivity versus radius (a) for a monolayer with refractive index $n_2 = 1.3$ and covering ratio $\Theta = 0.3$, (b) for $n_2 = 1.1$ and $\Theta = 0.1$, (c) for $n_2 = 1.5$ and $\Theta = 0.3$. MSM-M is the multiple-scattering model and SSA-M is the single-scattering approximation, both based on the Mie solution. EGL is the equivalent stratified layer and THF is a thin homogeneous film.

on the same radii for these two cases. EGL reflectivity oscillations heights decrease, which also happens to the scattering models, whereas the oscillations of the THF model have a constant height.

Qualitative relative results for other n_2 and Θ values are quite similar. For lower covering ratios and contrast—that is, for a lower refractive index difference $n_2 - n_1$—the SSE, MSM, and EGL plots are even closer, as shown in Fig. 4(b). In this case $n_2 = 1.1$ and $\Theta = 0.1$, SSA and MSM predictions are almost indistinguishable, and they get closer to the EGL plot but seem further away from THF. Again all four models are coincident up to $a \approx 0.1\lambda$, but SSA, MSM, and EGL keep close for a longer interval $a < 0.34\lambda$. For higher contrast, for example $n_2 = 1.5$ and $\Theta = 0.3$, shown in Fig. 4(b), SSE, MSM, and EGL reflectivities look different from each other, yet within the $a < 0.28\lambda$ range all three of them are still very similar.

2. Monolayer on a Plane Substrate

Reflectivity was also calculated for monolayers lying on a substrate; the surrounding medium refractive index is $n_1 = 1$, while the substrate is $n_3 = 1.5$. Particle radius a, refractive index n_2, and covering ratio Θ were varied. In Fig. 5(a), a typical graph is displayed, a monolayer with refractive index $n_2 = 1.3$ and covering ratio $\Theta = 0.3$—a combination that has been chosen in this work as a reference. Again the reflectivity predicted by the MSM, SSA, EGL, and THF models is shown. All models keep together for $a < 0.09\lambda$; THF departs first, EGL stays close to SSA for $a < 0.17\lambda$, and then they all behave differently. Reflectivity for the scattering models drops steadily as a increases due to extinction, but in THF and EGL cases, there is no extinction, so reflectivity oscillates around a constant mean value. When a substrate is present, the maximum and minimum reflectivity radii are closer for the scattering and EGL models.

For lower covering ratios and contrast, in this case $n_2 = 1.1$ and $\Theta = 0.1$, all reflectivity predictions are very similar for $a < 0.1\lambda$, but SSA, MSM, and EGL remain together for a longer interval $a < 0.2\lambda$; then the scattering models reflectivity drops due to extinction as shown in Fig. 5(b). Predictions for higher contrast and surface covering ratio, in particular $n_2 = 1.5$ and $\Theta = 0.3$, look very different from each other for $a > 0.125\lambda$ [Fig. 5(c)].

B. Comparison with Scattering Models under the Rayleigh–Gans Approximation

1. Free Standing Monolayer

Reflectivity was calculated for monolayers with different particle radii a, refractive indexes n_2, and surface covering ratios Θ using the SSA and MSM under the Rayleigh–Gans approximation. Reflectivity versus radius plots for the four models were drawn. In Fig. 6(a), a typical graph is displayed for a

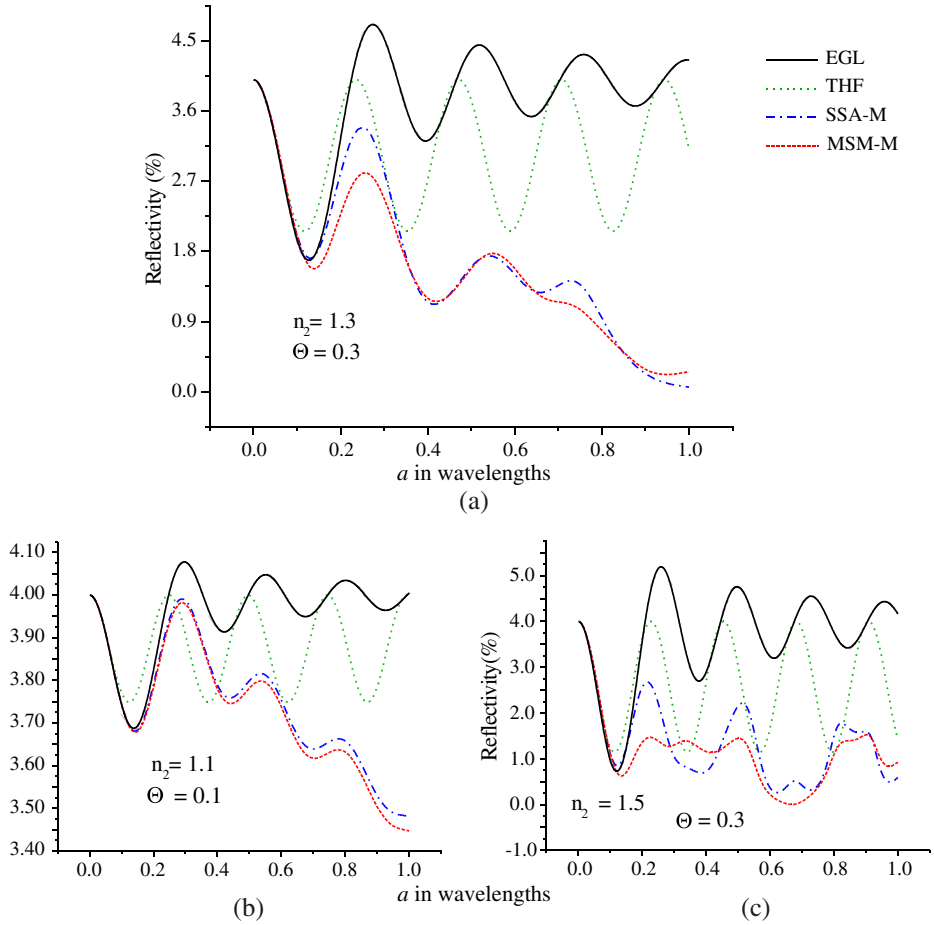

Fig. 5. (Color online) Reflectivity versus radius for a monolayer on a substrate with $n_3 = 1.5$. MSM-M is multiple-scattering model and SSA-M is single-scattering approximation, both based on the Mie solution. EGL is the equivalent stratified layer and THF is a thin homogeneous film. (a) The particles refractive index is $n_2 = 1.3$ and covering ratio is $\Theta = 0.3$; (b) $n_2 = 1.1$ and $\Theta = 0.1$; (c) $n_2 = 1.5$ and $\Theta = 0.3$.

monolayer with refractive index $n_2 = 1.3$ and covering ratio $\Theta = 0.3$. This time EGL and the scattering models reflectivity look surprisingly similar. SSA-R&G and MSM-R&G plots look almost identical. Strikingly the EGL prediction behaves slightly more like the scattering models based on the Mie solution than the one scattering approach (Rayleigh–Gans) to the other (Mie). Changing n_2 or Θ values basically scales the reflectivity on the vertical axis for SSA-R&G and MSM-R&G. The oscillation width is larger for SSA-R&G and MSM-R&G than for EGL this time, but if a subtle change was made in the size parameter definition, namely $x_m^{\text{new}} \equiv n_{\text{avg}} k_0 a$ instead of $x_m \equiv n_1 k_0 a$, oscillations would look almost identical for scattering models and EGL, as is evident from Fig. 6(b).

The overall behavior for other contrast values $n_2 - n_1$ and covering ratios Θ is similar. Again, as these values decrease, EGL and scattering model predictions approach each other. Conversely, as contrast and surface covering values rise, all differences grow as shown in Fig. 7. Still, SSA and MSM results present almost no difference between them under the Rayleigh–Gans approximation. Again, if the size parameter definition x_m is changed for x_m^{new}, the radii for the local maxima and minima are almost identical for the scattering models and EGL.

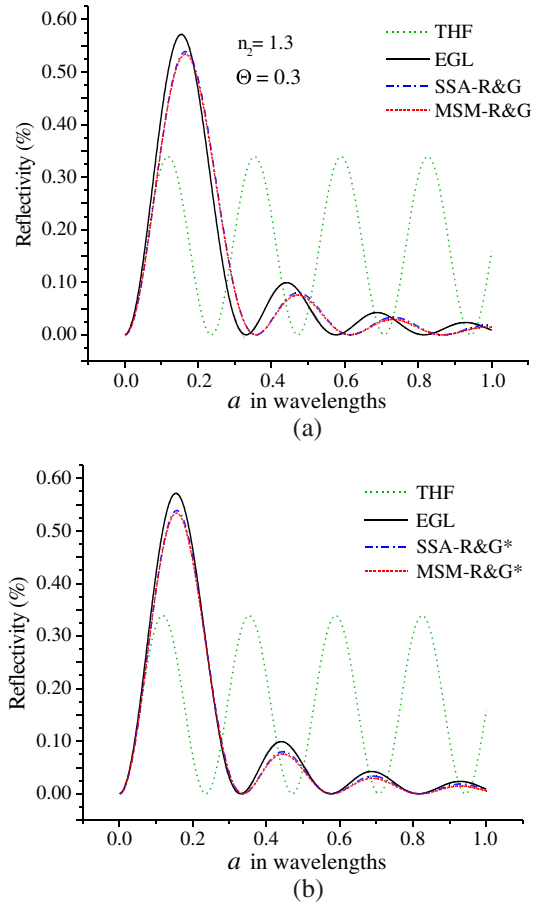

Fig. 6. (Color online) Reflectivity versus radius, for a monolayer with refractive index $n_2 = 1.3$ and covering ratio $\Theta = 0.3$. EGL is the equivalent stratified layer and THF is a thin homogeneous film. MSM-R&G is the multiple-scattering model and SSA-R&G is the single-scattering approximation, both in turn based on the Rayleigh–Gans approximation, (a) with the standard size parameter definition for scattering models $x_m \equiv n_1 k_0 a$ in Eq. (2), and (b) * with the new size parameter definition $x_m^{\text{new}} \equiv n_{\text{avg}} k_0 a$.

2. Monolayer on a Plane Substrate

Reflectivity was calculated for monolayers on a substrate; the surrounding medium refractive index is $n_1 = 1$, while the substrate is $n_3 = 1.5$. In Fig. 8(a), a typical graph is displayed, for a monolayer with refractive index $n_2 = 1.3$ and covering ratio $\Theta = 0.3$. The reflectivity plot for SSA climbs out of proportion as a grows, while MSM stays close to EGL, behaving very similarly but with slightly wider oscillations. Scattering of light under the Rayleigh–Gans approximation is very weak, so extinction is negligible, and consequently reflectivity does not drop steadily as particle size grows, as it happens when considering the Mie solution (Fig. 5). The fact that the transmission coefficient $t_{\text{coh}}^{\text{SSA}}$ in Eq. (5) yields transmissivities greater than 1, under the Rayleigh–Gans approximation, causes the reflectivity to rise.

The overall behavior for other contrast and covering ratio values is not so different. Once more, as these values drop, EGL and scattering models yield more similar results [Fig. 8(b)]. Conversely, as contrast and surface covering values rise, all differences grow [Fig. 8(c)].

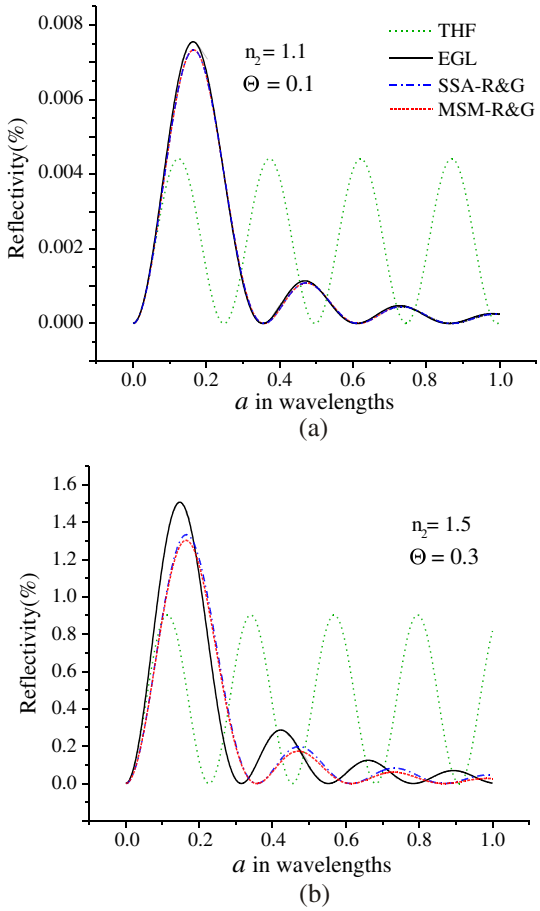

Fig. 7. (Color online) Reflectivity versus radius; MSM-R&G is the multiple-scattering model and SSA-R&G is the single-scattering approximation, both in turn based on the Rayleigh–Gans approximation. EGL is the equivalent stratified layer and THF is a thin homogeneous film, (a) for a monolayer with refractive index $n_2 = 1.1$ and covering ratio $\Theta = 0.1$, and (b) for a monolayer with $n_2 = 1.5$ and $\Theta = 0.3$.

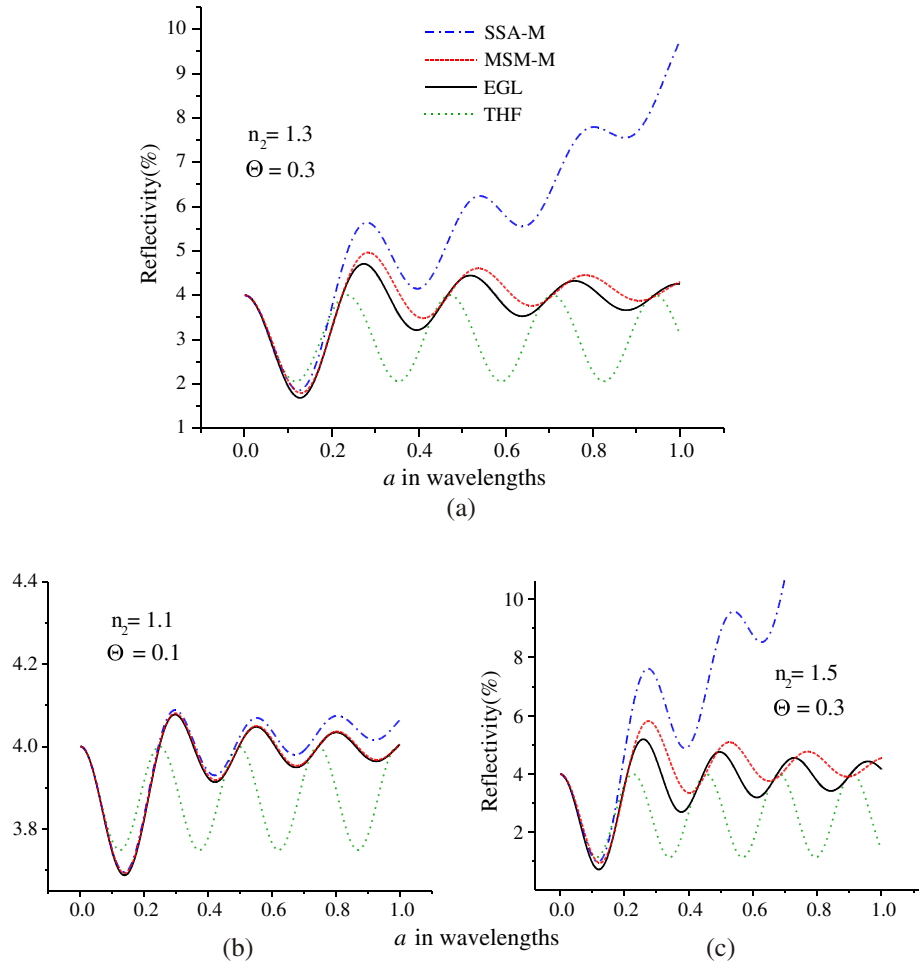

Fig. 8. (Color online) Reflectivity versus radius for a monolayer on a substrate with $n_3 = 1.5$. MSM-R&G is the multiple-scattering model and SSA-R&G is the single-scattering approximation, both in turn based on the Rayleigh–Gans approximation. EGL is the equivalent stratified layer and THF is a thin homogeneous film. (a) The particles refractive index is $n_2 = 1.3$ and covering ratio is $\Theta = 0.3$; (b) with $n_2 = 1.1$ and $\Theta = 0.1$, (c) with $n_2 = 1.5$ and $\Theta = 0.3$.

4. DISCUSSION AND CONCLUSIONS

A. Comparison with a THF

Although the THF is the simplest formulation of the problem and its reflectivity is expressed with an entirely analytical expression, it is accurate only for very small radii. In particular for reflectivity at normal incidence, modeling a random monolayer consisting of transparent spherical particles with a THF may be accurate for radii up to $a \sim 0.08\lambda$, judging from comparison made with the MSM-M. When a substrate is present, accuracy may extend to $a \sim 0.09\lambda$. The case for EGL looks better, and it behaves like the scattering models, SSA-M and MSM-M, for greater radius values, more so when there is no substrate.

B. Comparison with Scattering Models Based on the Mie Solution (SSA-M and MSM-M)

Scattering models based on the Mie solution are more accurate than the THF for greater radii since sizes and contrast are not restrained, but they lose accuracy for large covering ratios [8]. Yet, as particle radius grows, the number of terms in the Mie series needed for convergence grows as well. Although analytical, Mie type solutions are only known for certain particle shapes, namely spheres, ellipsoids, and infinite cylinders. The procedure followed here to get reflectivity results for an EGL is numeric, but the numerical method that solves the amplitude equation (15) for the EGL is less elaborate than the available Mie scattering software.

EGL is valid up to moderately small radii; details depend on the contrast and covering ratios, yet complexity of the numerical algorithm does not vary with size, contrast, or covering ratio. Any arbitrary but finite $n(z)$ profile can be inserted in Eq. (15); consequently, EGL allows easier treatment of nonspherical or irregular particles than scattering models based on Mie type solutions. If one would be interested in having an EGL analytical expression for the reflectivity $R(a)$, Eq. (14) can be solved in a power series for z, and then, with the appropriate initial conditions, reflectivity can be inferred [22].

Scattering models, SSA-M and MSM-M, present some differences between them too. SSA-M tends to higher reflectivities as n_2 and Θ values rise; in all these cases MSM-M is more reliable.

1. Suspended Monolayer

For a suspended monolayer, all three models—EGL, SSA, and MSM—either based on the Mie solution or even the Rayleigh–Gans approximation, predict a characteristic first reflectivity

boost as a increases from zero. Reflectivity first rises to a conspicuous maximum and then drops back. Looking at the reflectivity plots, it always seems that agreement between the EGL and scattering models deteriorates at end of this first "lump." From this observation, a validity range for the EGL can be inferred: $0 < a < g(n_2)$, where $g(n_2)$ appears to be a linear function of the refractive index n_2, namely $g(n_2) \approx (-0.16\lambda)n_2 + 0.51\lambda$. Within this radius range, EGL may even perform better than the scattering models for high covering ratios ($\Theta > 0.3$).

If we review carefully Eq. (11), we see that the difference between abscissas, corresponding to consecutive local extreme points, is related to the optical thickness difference between homogeneous layers [23]:

$$2n_{\text{avg}}(a_{m+1} - a_m) = \frac{1}{4}. \tag{18}$$

If we take a known average refractive index n_{avg} and calculate $a_1 - a_0$ with Eq. (18), corresponding to the first two local extrema, the effective thickness difference turns out to be smaller than the actual one. To see this, the THF plot may be used as a reference. The first reflectivity maximum, for the EGL and scattering models, corresponds to a greater radius than the first maximum for the THF; if a homogeneous layer criterion is used this would indicate a thinner optical thickness. The former observation may suggest that light is effectively reflected at planes closer to the monolayer center ($z_{\text{center}} = -a$) than its actual borders ($z_i = -2a$ and $z_f = 0$), when a is small ($a < 0.3\lambda$).

With increasing a values, reflectivity oscillations become narrower. In the EGL case, oscillation width tends to be the same as in the THF case; in the SSA-M and MSM-M cases, oscillation width becomes even smaller, and effective thickness differences would be greater than the actual ones for $a > 0.3\lambda$. Thin film reflectivity rises or drops depending on how light reflected at a first interface interferes with all successive reflections. The type of interference that take place depends on the phase lag between these successive reflections. A greater effective thickness difference may indicate a greater phase lag, which in turn may suggest that light takes slightly more time to come back out of a scattering monolayer consisting of big particles ($a > 0.3\lambda$) than a THF or a EGL. Apparently these back scattering particles "trap" light longer than the equivalent homogeneous or graded films.

The height of the first reflectivity maximum is smaller for THF than it is for EGL, SSA-M, and MSM-M. Reflectivity oscillation height is constant for THF since both reflecting planes at $z = -2a$ and $z = 0$ are perfect boundaries and it is a nonabsorbing film. The case for EGL is different. For a stratified medium, a smoother $n(z)$ function predicts a lower overall reflectivity [18,22,24]. Since the function $n(z)$ is smoother as a increases, EGL reflectivity oscillations height decreases, a feature that is present in scattering models too. For scattering models, this reflectivity oscillations height decrease is due to the α factor, which is proportional to a^{-2}, in Eqs. (4) and (6).

When dealing with a THF, Eq. (11) relates reflectivity oscillations maxima with the films refractive index [23]: $n_{\text{avg}} = n_1\left[\frac{(R_{\max})^{1/2}+1}{(1-R_{\max})^{1/2}}\right]$, where $R_{\max}$ is any reflectivity maximum. This suggests that, for reflection, a monolayer shows a greater effective refractive index than n_{avg} when $a \lesssim 0.3\lambda$.

2. Supported Monolayer

Scattering models treat the issue of a monolayer supported by a flat surface in three steps; first the reflection and transmission coefficients are found for the suspended monolayer, then with this data an equivalent plane is formulated and placed at some point z_1, and finally the substrate is added at some other point z_2. The EGL can treat all the $n(z)$ profile in only one procedure.

For a supported monolayer and $n_2 \leq 1.3$, the maximum and minimum reflectivity radii match better among EGL, SSA-M, and MSM-M. Quantitative agreement between EGL and the scattering models is good within the range $0 < a < h(n_2)$, where $h(n_2)$ also appears to be a linear function of the refractive index n_2: $h(n_2) \approx (-0.29\lambda)n_2 + 0.56\lambda$. Significant reflection takes place at the substrate surface. Overall reflectivity drops steadily with increasing a for SSA-M and MSM-M, which does not happen to the EGL. Extinction by scattering, the diffuse reflection component, is responsible for a lower reflectivity in the case of the scattering models. For $n_2 > 1.3$ and $a > 0.14\lambda$, scattering models produce a random-like result.

C. Comparison with Scattering Models Based on Rayleigh–Gans Approximation (SSA-R&G and MSM-R&G)

The main advantage of the Rayleigh–Gans approximation is that it yields very simple analytical expressions. The drawback is that Rayleigh–Gans approximation considers almost no extinction; a practically undisturbed plane incident wave upon the radiating dipoles and those dipoles do not interact. Under this approximation, propagation does not slow down when traveling through a denser medium.

Reflectivity predictions for an EGL and the scattering models (SSA-R&G and MSM-R&G) are strikingly similar, although there is enough difference between them to see that the EGL behavior is slightly closer to that of the scattering models based on the Mie solution and thus more reliable. Solving Maxwell equations for a stratified medium (EGL), in the case of normal incidence, yields plane waves too, although here, the interaction among all the dipoles that make up the medium is considered axiomatically and it is strongly coherent.

1. Suspended Monolayer

Reflectivity plots for EGL and scattering models depart from each other as contrast and covering ratio values grow. However, changing x_m for x_m^{new}, trying to account for a lower light propagation speed within the spheres, makes results look almost identical for EGL and scattering models.

2. Supported Monolayer

Single scattering yields transmission coefficients greater than 1 for the Rayleigh–Gans approximation, which makes reflectivity for a supported layer rise out of bounds when a increases. This is not the case for MSM-R&G; its reflectivity plot stays very close to the EGL's. Again, manipulating the size parameter by replacing n_1 for a slightly greater value, both plots can be matched and the remaining differences are very small.

D. Application to Experiment

It may seem that reflectivity versus particle radius plots are far from any experimental outcome; achieving a real monolayer

of identical spherical particles all growing in size simultaneously is difficult to imagine. Yet, as particle radius is given in terms of the wavelength in vacuum, varying the incident light frequency would be equivalent to changing the particle radius, although no dispersion is considered in this work. A spectrophotometer is the right device to generate reflectivity versus light frequency plots. For low contrast and moderately small particle sizes, the EGL model is more reliable than scattering models based on Rayleigh–Gans approximation, judging by the comparison made with scattering models based on the Mie solution. Biological samples tend to have low contrast, low covering ratios, and nonspherical symmetries, so in this case the EGL may be an excellent simple option to model reflectivity.

ACKNOWLEDGMENTS

We acknowledge financial support from Dirección General de Asuntos del Personal Académico from Universidad Nacional Autónoma de México through grant IN-106712 and from Consejo Nacional de Ciencia y Tecnología (Mexico) through grant 151137, "Conservation, invariants and wave propagation through inhomogeneous deterministic media."

REFERENCES

1. T. Yamaguchi, H. Takahashi, and A. Sudoh, "Optical behavior of a metal island film," J. Opt. Soc. Am. **68**, 1039–1044 (1978).
2. R. Lazzari, G. Renaud, C. Revenant, J. Jupille, and Y. Borensztein, "Adhesion of growing nanoparticles at a glance: surface differential reflectivity spectroscopy and grazing incidence small angle x-ray scattering," Phys. Rev. B **79**, 125428 (2009).
3. R. G. Barrera, M. del Castillo-Mussot, G. Monsivais, P. Villaseñor, and W. L. Mochán, "Optical properties of 2D disordered systems on a substrate," Phys. Rev. B **43**, 13819–13826 (1991).
4. T. Wenzel, J. Bosbach, F. Stietz, and F. Träger, "In situ determination of the shape of supported silver clusters during growth," Surf. Sci. **432**, 257–264 (1999).
5. T. Okamoto, I. Yamaguchi, and T. Kobayashi, "Local plasmon sensor with gold colloid monolayers deposited upon glass substrates," Opt. Lett. **25**, 372–374 (2000).
6. J. Toudert, D. Babonneau, L. Simonot, S. Camelio, and T. Girardeau, "Quantitative modelling of the surface plasmon resonances of metal nanoclusters sandwiched between dielectric layers: the influence of nanocluster size, shape and organization," Nanotechnology **19**, 125709 (2008).
7. R. Serna, J. C. G. de Sande, J. M. Ballesteros, and C. N. Afonso, "Spectroscopic ellipsometry of composite thin films with embedded Bi nanocrystals," J. Appl. Phys. **84**, 4509–4516 (1998).
8. A. García-Valenzuela, E. Gutiérrez-Reyes, and R. G. Barrera, "Multiple-scattering model for the coherent reflection and transmission of light from a disordered monolayer of particles," J. Opt. Soc. Am. A **29**, 1161–1179 (2012).
9. R. Diamant and M. Fernández-Guasti, "Light propagation in 1D inhomogeneous deterministic media: the effect of discontinuities," J. Opt. A **11**, 045712 (2009).
10. H. C. Van de Hulst, *Light Scattering by Small Particles* (Wiley, 1981).
11. C. F. Bohren and D. R. Huffman, *Absorption and Scattering of Light by Small Particles* (Wiley-Interscience, 1983).
12. M. Mishchenko, *Light Scattering by Nonspherical Particles. Theory, Measurements, and Applications* (Academic, 1999).
13. V. Bazhan, "ScatLab," http://www.scatlab.org.
14. V. A. Loiko, V. P. Dick, and V. I. Molochko, "Monolayers of discrete scatterers: comparison of the single-scattering and quasicrystalline approximations," J. Opt. Soc. Am. A **15**, 2351–2354 (1998).
15. M. C. Peña-Gomar, J. J. F. Castillo, A. García-Valenzuela, R. G. Barrera, and E. Pérez, "Coherent optical reflectance from a monolayer of large particles adsorbed on a glass surface," Appl. Opt. **45**, 626–632 (2006).
16. M. Born and E. Wolf, *Principles of Optics* (Cambridge University, 2005).
17. E. Hecht Eugene, *Optics* (Addison Wesley, 2002).
18. M. Fernández-Guasti, A. Gil-Villegas, and R. Diamant, "Ermakov Equation Arising from Electromagnetic Fields Propagating in 1D Inhomogeneous Media," Rev. Mex. Fís. **46**, 530–538 (2000).
19. J. L. Reid and J. R. Ray, "Ermakov systems, nonlinear superposition and solutions of nonlinear equations of motion," J. Math. Phys. **21**, 1583–1587 (1980).
20. P. B. Espinoza-Padilla, "Ermakov-Lewis dynamic invariants with some applications," http://arxiv.org/pdf/math-ph/0002005.
21. N. Atzin, M. Fernandez–Guasti, and R. Diamant, "Light propagation at soft interface," http://demonstrations.wolfram.com/LightPropagationAtSoftInterface/.
22. P. S. Epstein, "Reflection of waves in an inhomogeneous absorbing medium," Proc. Natl. Acad. Sci. USA **16**, 627–637 (1930).
23. A. M. Goodman, "Optical interference method for the approximate determination of refractive index and thickness of a transparent layer," Appl. Opt. **17**, 2779–2787 (1978).
24. R. Jacobsson, "Light reflection from films of continuously varying refractive index," in *Progress in Optics*, *Vol. V*, E. Wolf, ed. (North-Holland, 1966), pp. 248–286.